Accepted Manuscript

Photocatalytic degradation of naphthalene using calcined Fe-ZnO/ PVA nanofibers

Aiswarya Devi Sekar, Harshiny Muthukumar, Nivedhini Iswarya Chandrasekaran, Manickam Matheswaran

Please cite this article as: Sekar, A.D., Muthukumar, H., Chandrasekaran, N.I., Matheswaran, M., Photocatalytic degradation of naphthalene using calcined Fe-ZnO/ PVA nanofibers, *Chemosphere* (2018), doi: 10.1016/j.chemosphere.2018.04.131.

1 **Photocatalytic degradation of naphthalene using calcined Fe-ZnO/ PVA**

2 **nanofibers**

3 Aiswarya Devi Sekar, Harshiny Muthukumar, Nivedhini Iswarya Chandrasekaran, Manickam

4 Matheswaran*

5 Department of Chemical Engineering, National Institute of Technology, Tiruchirappalli,

6 India-620 015

7 *** Corresponding author email ID: matheswaran@nitt.edu**

8 **Graphical Abstract**
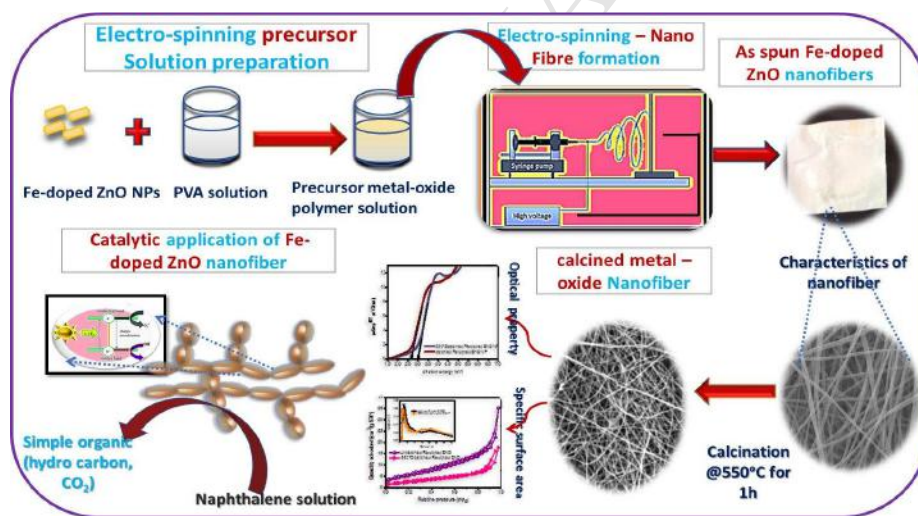
11 **Synopsis: Facile fabrication of Fe- ZnO/PVA nanofibers for photocatalytic degradation of**

12 **naphthalene.**

ABSTRACT:

Recently, the incorporation of metal oxide nanoparticles into polymers has gained great attention owing to their ample of applications. The green mediated synthesis Fe-doped ZnO nanoparticles have been incorporated into PVA nanofibers through electro spinning for the application of photocatalytic degradation. The PVA polymer concentration was optimized to obtain uniform fibers without beads. The Fe-doped ZnO nanofibers were characterized by various analyzing techniques. The results show that good physicochemical with high surface area, uniformity in fiber with an average diameter ranges from 150-300 and 50-200nm for un-calcined and calcined Fe-doped ZnO nanofiber respectively. The photocatalytic activity of nanofibers was examined by the degradation of naphthalene. The efficiency was observed 96 and 81% for calcined and un-calcined nanofibers, respectively. The reusable efficacy of Fe-doped ZnO calcined nanofiber as a catalyst was studied. These studies corroborated that the calcined Fe-doped ZnO nanofiber as promising material for catalytic applications.

Keywords: electrospinning, nanofiber, calcination, naphthalene, and degradation.

HIGHLIGHTS

- ➢ Synthesis of Fe-doped ZnO/PVA nanofibers with good physicochemical properties.
- ➢ Optimization and calcination of nanofibers to enhance the degradation capacity.
- ➢ Calcined nanofiber has showed better photocatalytic degradation activity than Un-calcined Fe-doped ZnO/PVA nanofiber.
- ➢ Reusability study has delineated the stability of Fe-doped ZnO nanofiber.

1. INTRODUCTION

35   The contamination of numerous water bodies in the environment is due to discharge of

36   several pollutants from rapidly growing industries and urbanization (Mahmoodi and Mokhtari-

37   Shourijeh, 2015; Karak et al., 2013). As per WHO Progress on drinking water, 2017 update and

38   SDG baselines, 844 million people still lacked even a basic drinking water service. Hence, the

39   eternally increasing drinking water demand has laid stress on the removal of azo dyes, heavy

40   metals and toxic organic pollutants from water (Liu et al., 2012; Wan et al., 2016; Hu et al., 2016

41   Wan et al., 2018). Among the toxic organic water pollutants, polycyclic aromatic hydrocarbons

42   (PAHs) are highly hazardous (Mondal et al., 2014; Wang et al., 2009). PAHs are typical

43   carcinogenic and mutagenic pollutants found in urban runoff that result from anthropogenic

44   activities (Rezvani-Eivari et al., 2016; Reddy et al., 2013). Naphthalene is one among the 16

45   toxic PAHs listed by Environmental Protection Agency (EPA) of the US and the European

46   Union. Since naphthalene possess higher water solubility and toxicity causes kidney damage,

47   congenital abnormalities and cancer in human beings (Mondal et al., 2014; Felix et al., 2014;

48   Zelinkova and Wenzl 2015). Jia and Batterman (2010) have deliberated that, NIOSH's

49   permissible exposure limit and ACGIH's threshold limit value of naphthalene as 50 $\mu g/m^3$, but it

50   has faced much higher than the threshold limit levels in the environment. Several conventional

51   practices have attempted and acquired only little effect on eliminating naphthalene, due to its

52   stability and strong recalcitrant nature (Luo et al., 2015).

53   Lair et al. (2008) have declared photocatalytic degradation as cheaper as and faster than

54   many existing possible techniques such as bioreactors, ozonolysis, pulse radiolysis and electron

55   beam irradiation etc. for removing pollutants. Similarly Gutierrez-Mata et al. (2017) described

56   the photocatalytic process as less toxic and low cost due to mineralization of the toxic organic

57   contaminants completely into less toxic or CO_2 and H_2O. Owing to their high catalytic activity

58   and large surface area, nanoparticles (NPs) have been explored broadly in the field of

59   photocatalytic degradation of PAH as well as disinfection (Dong et al., 2015). Farhadian et al.

60   (2016) evaluated the degradation of naphthalene using WO_3-MWCNT nanocomposite in visible

61   light. TiO_2 Degussa P-25 investigated as a semiconductor photocatalyst for degradation of

62   naphthalene in aqueous solution. Lin et al. (2009) achieved the degradation efficiency of 93.5%

63   for naphthalene within 120 min under visible light irradiation using La-N-TiO_2/AC

64   photocatalyst. Muthukumar et al. (2017) evaluated the degradation efficiency of naphthalene

65   using 40ppm of ZnO and Fe-doped ZnO NPs and affirmed Fe-doped ZnO exhibits more

66   degradation than pure ZnO NPs. Nair et al. (2011) described ZnO and Co-doped ZnO NPs

67   exhibits good photocatalytic activity. Sood et al. (2016) confirmed the wide range of

68   semiconductor metal oxides, ZnO exhibits good photocatalytic activity in agreement. The

69   cytotoxicity, antimicrobial and photocatalytic activity of ZnO and Fe-doped ZnO NPs were

70   evaluated successfully and obtained better results for Fe-doped ZnO than pure (Devi et al.,

71   2017). The strong tendency of agglomeration and difficulties in separation of NPs decreases the

72   photocatalytic degradation activity of pollutants in the aqueous state. In recent times, one

73   dimensional (1D) metal oxide nanofibers (NF) have received much attention due to its promising

74   surface morphology, essential for catalyst applications such as large surface area and porous

75   structure (Wang et al., 2017; Liu et al., 2008; Malwal and Gopinath 2017). Various researchers

76   stated that polymeric NF in the form of a matrix, protect the inorganic NPs from agglomeration,

77   control the particle size and their distribution, and make the separation process of utilized

78   composite NF more convenient (Panthi et al., 2017, Park and Lee 2014). Wang et al. (2017)

79   described the porous structure of NF enhances the ability of metallic NPs to disperse and stable

80   in aqueous solutions.

81   Electrospinning is a simple, less expensive and very popular technique for fabricating

82   continuous NF among the several methods of NF such as electrochemical deposition, layer-by-

83   layer self-assembly and template-assisted techniques (Shahini et al., 2016; Singh et al., 2013; An

84   et al., 2014; Mishra and Ahrenkiel, 2012). The intrinsic properties of NF such as large surface

85   area, increased shelf-life, better chemical stability and higher porosity, makes them more suitable

86   for water treatment applications (Samadi et al., 2012; Panthi et al., 2017; Park and Lee 2014).

87   Therefore, electrospun NF are potential candidate for a wide range of applications such as

88   catalysis (Mondal, 2017), sensors (Bai et al., 2014), adsorption (Wang et al., 2014), disinfection

89   (Si et al., 2017; Galkina et al., 2015), tissue engineering scaffolds (Croisier and Jérôme, 2013;

90   Agarwal et al., 2008) and filtration (Choi et al., 2015). Many studies reported the successful

91   incorporation of semiconductors (metal oxides) in various polymer NF using electrospinning

92   processes (Panthi et al., 2017; Singh et al., 2013). Wang et al. (2016) stated the enhanced

93   photocatalytic activity of degrading organic pollutant using N-decorated and Mn^{2+} doped ZnO

94   NF. Singh et al. (2013) been demonstrated the efficacy of the mats, incomplete degradation of

95   naphthalene and anthracene dyes in the wastewater treatment. Mondal et al. (2015) confirmed

96   the photocatalytic degradation of naphthalene using Optimized free-standing mesoporous anatase

97   TiO_2 NF mats fabricated by electrospinning.

98   With this insight, the Fe-doped ZnO NPs incorporated nanofiber was fabricated by

99   electrospinning. The photocatalytic degradation of naphthalene was investigated. The polymer

100   concentration was optimized to obtain smooth and uniform NF. The physico-chemical traits of

101   synthesized NFs were analyzed using various analytical instruments. The photocatalytic

102   degradation efficiency of un-calcined and calcined Fe-doped ZnO NF were evaluated using

103   naphthalene under UV irradiation.

2. EXPERIMENTAL

2.1 Materials

The chemicals such as Ferric chloride ($FeCl_3$), Zinc nitrate ($Zn\ (NO_3)_2$), Polyvinyl alcohol (PVA), Sodium hydroxide (NaOH), Hydrochloric acid (HCl) and Ethanol were purchased from Merck and Himedia India. Milli-Q water (18.20MΩ cm resistivity) was used for all the experiments. All the chemicals were used as received, without any further purification.

2.2 Synthesis of Fe-doped ZnO NPs

Green mediated Fe-doped ZnO NPs were synthesized using *A. spinosus* leaf extract. The hydro-alcoholic leaf extract of *A. spinosus* was carried out using soxhlet apparatus and stored at 5°C. 10 mg of extract was taken and dissolved in 100 mL of deionized water and used as a reducing agent for NPs synthesis. For synthesis of Fe-doped ZnO NPs, an aqueous solution of 1.0M $ZnNO_3$ and $FeCl_3$ were prepared. The pH of solution was adjusted using 0.1 N HCl and 0.1 N NaOH. The Zn and Fe precursor solutions were mixed and equivalent amount of leaf extracts (pH 9) was added drop-wise with stirring at 37 ± 1°C for 45 min. The reddish white Fe-doped ZnO precipitates were filtered and washed. The sample was dried in oven at 100 °C for 4 h. The dried material was powdered in a mortar-pestle and used for further study.

2.3 Fabrication of Fe-doped ZnO/PVA composites NF

The preparation electrospinning precursor solutions were as follows; 4, 8 and 12 wt. % PVA solution was prepared by dissolving PVA salt in distilled water with a vigorous stirring at 7000 rpm at 70 ºC for 2.0 h to attain a uniform translucent solution. The synthesized Fe-doped ZnO NPs was added to PVA solutions and mixed together to obtain homogenous suspension in magnetic stirrer with vigorous stirring for 4 h at room temperature. The 4 wt. % of Fe-doped ZnO NPs were used for the fabrication of the composite NF.

127 The Electrospinning technique was used for the fabrication of Fe-doped ZnO NPs/PVA

128 composite NF. The homogenous polymer solution was loaded in a syringe equipped with an 18

129 gauge stainless steel needle connected to an electrode of a high voltage power supply and the

130 grounded electrode was an aluminum foil (wrapped on the aluminum plate) used as a collector.

131 The optimized parameters used to produce NF through electrospinning are as follows: distance

132 from the needle tip to the collector was 12 cm, 0.3 mL/h of the solution was fed to the needle tip

133 with the applied high voltage of 17 kV between the needle tip and the grounded collector. NF got

134 deposited on the aluminum foil were separated after the completion of electrospinning process.

135 All the experiments were executed at room temperature. The as-spun NF were dried in vacuum

136 for 48 h to eliminate the remaining solvent and then stored in the desiccator for further

137 characterizations. The calcination of NF were carried out at 550 ºC for 1 h.

138 **2.4 Characterization of the NFs**

139 The morphology of the composite NFs were characterized by scanning electron

140 microscopy (SEM, JEOL Model JSM - 6390LV). Prior to SEM examination, a thin layer of Au

141 was sputter-coated on the samples in order to prevent abnormal charging. Verification of the Fe-

142 doped ZnO NPs distribution in the PVA NF was confirmed by a JEOL transmission electron

143 microscope with an acceleration voltage of 15 kV at high vacuum. For Transmission electron

144 microscopy (TEM, 200 KV FEI-Tecnai G2 20 S) specimen preparation, the fiber was collected

145 by placing a small copper grid under the electrospinning nozzle for 10 s during the

146 electrospinning process. The transmission electron micrographs and selected area electron

147 diffraction (SAED) patterns of NF were captured using FEI TECHNAI G2 and JEOL 2100

148 UHR-TEM operating at 200 KV with machine resolution of 0.4 nm. The X-ray diffraction

149 (XRD) data were obtained by Rigaku Ultima III by step scan technique with Cu-Ka radiation

150 (1.500 A, 40 kV, 30 mA) in the range of 10–80º at a scan rate of 0.5º /min. Thermo gravimetric

151 analysis (TGA) of electrospun NF was conducted on a Perkin Elmer STA 6000, Diamond

152 TG/DTA thermal analyzer by heating them up to the temperature 800º C with a heating rate of

153 10º/min in the presence of flowing air (200 mL/min). Infra-red Spectra (FTIR) of NF were

154 recorded using (FTIR- Thermo Scientific99 ™ Inc. Nicolet™ iS™5) with a spectral range of

155 400-4000 cm^{-}1. The Brunauer–Emmett–Teller (BET) surface area was analyzed using nitrogen

156 adsorption on a Micromeritics ASAP 2020 nitrogen adsorption apparatus. Prior to analysis, the

157 sample was degassed under vacuum at 150º C for 7 h.

158 **2.5 Photocatalytic Experiment**

159   The photocatalytic activities of electrospun NF have been examined for photolysis,

160 adsorption, and degradation of 40 ppm naphthalene solution under various conditions. The

161 experiments were carried out in a beaker with the magnetic stirrer under UV light of 16 W;

162 initially, 500 mL of naphthalene solution without catalyst was exposed to UV light. In the

163 control experiment, fabricated NF catalysts were loaded to naphthalene solution in the absence of

164 UV light. Then finally, 30 mg of Fe-doped ZnO NPs, calcined and un-calcined Fe-doped

165 ZnO/PVA NF were added to 500 mL of 40 ppm naphthalene solutions in different beakers and

166 exposed to UV light. The solutions were continuously exposed to UV light maintained at 37 ± 1

167 ºC for 4 h. At the regular interval of time, samples were collected to monitor the reaction and the

168 used photocatalyst was removed in prior to analysis. The naphthalene degradation was assessed

169 using UV-visible spectrophotometer with a wavelength range of 200-700 nm. The photocatalytic

170 degradation efficiency for naphthalene was calculated using the following equation,

171 Percentage of degradation= $(A_0 - A_t)/A_0 * 100$

172   Where A_0 and A_t is the absorbance of the initial concentration and after the time ('t') of

173   naphthalene solution. The reusability of NF was analyzed to study the stability of electrospun

174   NF.

175   **3. RESULTS AND DISCUSSION**

176   **3.1 Morphological Analysis of NF**

177   SEM micrographs of Fe-doped ZnO/PVA NFs has shown in the Fig.1, which illustrates

178   the variation in morphology of NFs with an increase in PVA concentration. The polymer

179   concentration was optimized between 4, 8 and 12 wt. % to obtain uniform beadless NFs with

180   diameters ranging from 200–300 nm. Fig 1 (a) and (b) shows the morphology and histogram of 4

181   wt. % of PVA composite NF with an average smaller diameter of 188 nm, which having beads.

182   But 8 wt. % of PVA composite NF delivered the beadless, smooth and uniform average 219 nm

183   diameter were shown in the fig 1 (c) and (d), respectively. The reduction of beads and increased

184   uniformity was due to high viscoelasticity with the increase of polymer concentration (Singh et

185   al., 2013). Also, smoothness of NF was owing to PVA, it acted as a template and provides

186   appropriate viscosity to make the solution electro-spinnable (Malwal and Gopinath, 2016). Then

187   the 12wt. % of PVA concentration in Fig 1 (e) and (f) offered the beadless, broader NF with an

188   average diameter of 481 nm. This is ascribed to increase in viscosity of electrospinning solution

189   (Imran et al., 2013). Therefore, from the results 8 wt. % of PVA was obtained as optimum for

190   this study. Fig 2 (a) and (b) presents the SEM micrograph and histogram of calcined Fe-doped

191   ZnO with the porous surface and average diameter ranges from 50 to 200 nm. It is apparent that

192   the thermal treatment significantly changes the morphological properties of the as-spun material

193   (Busuioc et al., 2015). Smooth and uniform surfaces of as–spun composite nanofibers have been

194   modified as a result rough, porous with shrinkages, reduced diameter, and crystallization of an

195 oxide phase in the form of nanometric grains during calcination due to the decomposition of

196 PVA component (Viswanathamurthi et al., 2003). Subsequently, the hierarchical structures or

197 nanotexturing provided by the electrospun nanofiber significantly enhance the surface-to-volume

198 ratio, thereby giving rise to improved photocatalytic activity (Li et al., 2015; An et al., 2014).

199 Further characterization studies were done with 4 wt. % of Fe-doped ZnO NPs incorporated in 8

200 wt. % of PVA polymer precursor solution.

3.2 Structural Analysis

202 The structural information of before and after calcination of NFs were obtained by XRD

203 analysis. Fig 3 (b) showed the pattern of as-spun Fe-doped ZnO /PVA NFs with 2θ diffraction

204 peaks at 19.6° corresponds to (101) plane of semi-crystalline PVA (Judy et al., 2012). The

205 remaining 2θ peaks at 31.9º, 34.1º, 36.2º, 44.6º, 56.4º and 62.6º corresponds to (100), (002),

206 (101), (102), (110) and (103) crystal planes of Fe-doped ZnO (JCPDSno:01-079-0207)

207 (Muthukumar et al., 2017; Baranowska-Korczyc et al., 2013). The diffraction pattern of calcined

208 composite NF was displayed in Fig 3 (c). All the peaks of calcined NF were highly sharp and

209 intensified than as-spun, this denoted the highly crystalline nature of NF and disappearance of

210 PVA peak was asserted to the complete removal of the polymeric compounds leaving behind

211 pure crystalline in NF. Thus the XRD results evidently confirmed the removal polymer and

212 crystalline nature of Fe-doped ZnO NPs in the calcined composite NF. Fig. 4 displays the band

213 gap of calcined and un-calcined Fe-doped ZnO NF. The value of band gap increased for calcined

214 NF when compared to uncalcined NF. This might be due to change in the crystal size during the

215 calcination (Malwal and Gopinath, 2017).

3.3 Thermo Gravimetric Analysis

217   Fig.5 demonstrates the thermal behaviors of the as-spun NFs, investigated by thermo

218   gravimetric analysis. The thermograph of pure PVA showed the initial weight loss below 190 ºC

219   which corresponds to moisture loss, and then subsequent weight loss occurred at 250–350 ºC due

220   to decomposition of the polymeric side chains in PVA and the final weight loss occurred in the

221   range of 390–530 ºC which denotes the cleavage of C-C bonding in the polymer (Gong et al.,

222   2014). whereas the Fe-doped ZnO/PVA NF exhibited initial weight loss of 10 wt. % at 180 ºC

223   which corresponds to the loss of water molecules and the second weight loss of 68 wt. % was

224   observed between 230-420 ºC might be due degradation of organic compounds (Fernandes et al.,

225   2011). Followed by the degradation of PVA linkages and about 4wt. % of the residue was

226   detected between the ranges of 430-540 ºC (Hallaji et al., 2015). After that, no major change was

227   found with the rise in temperature represents the presence of inorganic compounds. Hence it has

228   confirmed the calcination temperature is above 540 ºC, also this variance in weight percent

229   between pure PVA and composite NF clearly suggested the successful incorporation of Fe doped

230   ZnO NPs in PVA NF.

231   **3.4 FTIR Analysis**

232   FTIR analysis was carried to examine the vibrational peaks of electrospun NF. Fig. 6

233   presents the FTIR spectra for as-spun pure PVA, Fe-doped ZnO/PVA, and calcined Fe-doped

234   ZnO NFs. Fig. 6 (a) and (b) stated the observation of strong peaks in as-spun pure PVA and Fe-

235   doped ZnO/PVA NF at 3304, 2930, 1708, 1421, 1328, 1090 and 838 cm^{-1} agrees well to PVA

236   molecules (Huang et al., 2016). The broad FTIR band at 3304 was identified as O-H stretching

237   vibration, then the peaks at 2930 and 1708 cm^{-1} were assigned to the (-CH_2-) bending and

238   vibration of (-C=O), respectively. The peaks appeared at 1421 and 1328 cm^{-1} were attributed to

239   bending of (CH_2-) and stretching of nitrile group (-CN-), respectively (Li et al., 2017). The small

11

240   peaks obtained at 1090 and 838 cm^{-1} were corresponds to O– C– O vibration of the acetal and –

241   CH group, respectively. Besides a strong absorption peak found in as-spun composite NF alone

242   at 587 cm^{-1} belongs to the Fe-doped ZnO (Muthukumar et al., 2017). Fig.6 (c) unveiled the FTIR

243   spectra of calcined NF with a single peak at 587 cm^{-1} belongs to the Fe-doped ZnO. All the

244   remaining peaks correspond to water molecules and organic substances were disappeared in the

245   calcined NF (Malwal and Gopinath, 2017; Imran et al., 2013). Thus the FTIR spectra clearly

246   elucidate the vibrational peaks pertaining to Fe-doped ZnO in as-spun NF and complete removal

247   of the polymer leaving behind the inorganic in calcined Fe-doped ZnO NF

3.5 BET Surface Area Analysis

249   The Brunauer– Emmett–Teller (BET) analyses of the samples have exhibited the surface

250   area of uncalcined and calcined Fe-doped ZnO NF as 38.5 and 17.8m^2/g, respectively were

251   shown in Fig.7. It also depicts the type IV curve accompanied by a type H3 hysteresis loop,

252   which is attributed to the predominance of mesopores (Bai et al., 2014). The pore size

253   distributions were measured by the Barret–Joyner–Halenda (BJH) method (Liang et al., 2015);

254   both the samples showed the average pore diameter 2.8 ± 2 nm were shown in the inset of Fig7.

255   The pore volumes of the un-calcined and calcined Fe-doped ZnO NF were 0.113cc/g and

256   0.026cc/g. Thus, the results indicate a mixture of micro and mesoporous nature of fabricated NF.

3.6 Photocatalytic degradation of naphthalene

258   Photocatalytic activities of 4 wt. % of un-calcined and calcined Fe-doped ZnO/PVA NF

259   were examined and compared with control experiments. Initially, photolysis was carried out on

260   40 ppm of naphthalene at pH 7 followed with the presence of a catalyst for 4 h in dark as a

261   control. Fig. 8 depicts the degradation efficiency of the catalyst under different experimental

12

262   conditions. 15% of naphthalene degradation was observed in photolysis, whereas 60 ppm of ZnO

263   NPs, Fe-doped ZnO NPs, calcined and un-calcined Fe-doped ZnO/PVA NF under dark condition

264   were exhibited 36, 45, 58, and 80%, respectively. This increase in degradation efficiency under

265   dark condition was attributed to adsorption of naphthalene on the surface of NPs and NFs

266   (Farhadian et al., 2016; Mondal et al., 2014). Finally, in the presence of UV light 58, 70, 81 and

267   96% of naphthalene degradation efficiencies were obtained for ZnO NPs, Fe-doped ZnO NPs,

268   un-calcined and calcined Fe-doped ZnO/PVA NF, respectively. This was due to Fe doping of

269   photocatalyst could improve the degradation efficiency by band gap narrowing, forming impurity

270   energy levels and oxygen vacancies, they act as electron accepters to trap electrons and

271   interstitial oxygen act as shallow trappers for holes both prevent the recombination of

272   photogenerated electrons and holes, thereby increasing the efficiency (Li et al., 2015). In

273   addition the nano-texturing provided by the calcined nanofiber significantly enhance the surface-

274   to-volume ratio, thereby giving rise to improved photocatalytic activity (Busuioc et al., 2015).

275   Calcination has increased the surface morphology of nanofibers (Li et al., 2015). The

276   naphthalene degradation efficiency of ZnONPs<Fe-doped ZnO NPs <un-calcined Fe-doped

277   ZnO/PVA NF <calcined Fe-doped ZnO NF under UV light irradiation at pH 7. Thus the results

278   corroborated calcined Fe-doped ZnO showed better degradation efficiency than other

279   nanocatalysts

280   The recyclability of calcined Fe-doped ZnO/PVA NF was checked for consequent five cycles

281   with the same photocatalyst and the fresh naphthalene solution was taken after every cycle. Fig.

282   9 displays the photocatalytic efficiency of NF up to five cycles. Initially, up to three cycles no

283   significant reduction was observed, beyond the 3rd cycle slight reduction of efficiency was found.

284 The virtuous recyclability of calcined Fe-doped ZnO NF was revealed from the above results.

285 Hence the calcined Fe-doped ZnO NF can be used for various water remedial applications

286 **4. Conclusions**

287 The Fe-doped ZnO NPs incorporated PVA NFs were successfully fabricated using

288 electrospinning. The PVA polymer concentration was optimized as 8 wt. % to obtain a uniform,

289 smooth nanofiber with an average diameter of 200 ± 10 nm before calcination. The post-

290 treatment of calcination at 550 ºC for 1 h showed porous NFs with diameters of 120 ± 10nm and

291 surface area lesser than un-calcined Fe-doped ZnO/PVA NFs. The characterization of results

292 NFs also confirmed the possession of uniform diameters with the large surface area. The band

293 gap of calcined was more than un-calcined nanofibers. The photocatalytic activity of naphthalene

294 degradation delineated that, calcined Fe-doped ZnO NFs exhibited good degradation efficiency

295 than un-calcined Fe-doped ZnO/PVA NFs. In addition, the reusability study revealed the stability

296 of calcined Fe-doped ZnO NFs. Thus the electrospinning of metal oxide incorporated NFs can be

297 truly suggested as a promising material for various photocatalytic applications in water

298 remediation process.

303 **REFERENCES**

304   1. Agarwal, S., Wendorff, J H., Greine, A., 2008. Use of electrospinning technique for

305   biomedical applications. Polymer.49, 5603-21.

14

306   2. An, S., Joshi, BN., Lee, MW., Kim, NY., Yoon, SS., 2014. Electrospun graphene-ZnO

307   nanofiber mats for photocatalysis applications. Appl. Surf. Sci.294, 24-8.

308   3. An, S., Joshi, BN., Lee. M W., Kim, N Y., Yoon, SS., 2014. Electrospun graphene-ZnO

309   nanofiber mats for photocatalysis applications. Appl. Surf. Sci. 294, 24-8.

310   4. Bai, S., Chen, S., Zhao, Y., Guo, T., Luo, R., Li, D., Chen, A., 2014. Gas sensing

311   properties of Cd-doped ZnO nanofibers synthesized by the electrospinning method. J.

312   Mater. Chem. A. 2, 16697-706.

313   5. Baranowska-Korczyc, A., Fronc, K., Pełka, J B., Sobczak, K., Klinger, D., Dłużewski, P.,

314   Elbaum, D., 2013. Structural studies of magnetic Fe doped ZnO nanofibers. Radiat. Phys.

315   Chem. 93, 21-4

316   6. Busuioc, C., Evanghelidis, A., Enculescu, M., Enculescu, I., 2015. Optical and

317   photocatalytic properties of electrospun ZnO fibers. Dig J Nanomater Biostruct.10, 957 –

318   965.

319   7. Choi, J., Yang, B J., Bae, G N., Jung, J H., 2015 Herbal extract incorporated nanofiber

320   fabricated by an electrospinning technique and its application to antimicrobial air

321   filtration. ACS Appl. Mater. Interfaces. 7, 25313-20.

322   8. Croisier, F., Jérôme, C., Chitosan-based biomaterials for tissue engineering. Eur. Polym.

323   J. 2013, 49, 780-92.

324   9. Devi, S A., Harshiny, M., Udaykumar, S., Gopinath, P., Matheswaran, M., 2017. Strategy

325   of metal iron doping and green-mediated ZnO nanoparticles, dissolubility, antibacterial

326   and cytotoxic traits. Toxicol Res. 6, 854-65.

327   10. Dong, S., Feng, J., Fan, M., Pi, Y., Hu, L., Han, X., Liu, M., Sun, J., Sun, J., 2015.

328   Recent developments in heterogeneous photocatalytic water treatment using visible light-

329   responsive photocatalysts, a review. RSC Adv. 5, 14610-30.

330   11. Farhadian, M., Sangpour, P., Hosseinzadeh, G., 2016. Preparation and photocatalytic

331   activity of WO$_3$–MWCNT nanocomposite for degradation of naphthalene under visible

332   light irradiation. RSC Adv. 6, 39063-73.

333   12. Felix, A., Amenaghawon, A., Mededode A., 2014. Heterogeneous photocatalytic

334   degradation of naphthalene using periwinkle shell ash, effect of operating variables,

335   kinetic and isotherm study. S. Afr. J. Chem. Eng. 19, 31-45.

336   13. Fernandes, D M., Hechenleitner, A W., Lima, S M., Andrade, L H., Caires, A R., Pineda,

337   E G., 2011. Preparation, characterization, and photoluminescence study of PVA/ZnO

338   nanocomposite films. Mater. Chem. Phys. 128, 371-6.

339   14. Galkina, O L., Önneby, K., Huang, P., Ivanov, V K., Agafonov, A V., Seisenbaeva, G A.,

340   Kessler, V G., 2015. Antibacterial and photochemical properties of cellulose nanofiber–

341   titania nanocomposites loaded with two different types of antibiotic medicines. J. Mater.

342   Chem. B. 3, 7125-34.

343   15. Gong, X., Tang, C Y., Pan, L., Hao, Z., Tsui, C P., 2014. Characterization of poly (vinyl

344   alcohol)(PVA)/ZnO nanocomposites prepared by a one-pot method. Composites Part B,

345   Engineering. 60, 144-9.

346   16. Gutierrez-Mata, A G., Velazquez-Martínez, S., Álvarez-Gallegos, A., Ahmadi, M.,

347   Hernández-Pérez, J A., Ghanbari, F., Silva-Martínez, S., 2017. Recent Overview of Solar

348   Photocatalysis and Solar Photo-Fenton Processes for Wastewater Treatment. INT J

349   PHOTOENERGY. https://doi.org/10.1155/2017/8528063

350   17. Hallaji, H., Keshtkar, A R., Moosavian, M A., 2015 A novel electrospun PVA/ZnO

351   nanofiber adsorbent for U (VI), Cu (II) and Ni (II) removal from aqueous solution. J

352   Taiwan Inst Chem Eng. 46, 109-18.

353 18. Hu, L., Zeng, G., Chen, G., Dong, H., Liu, Y., Wan, J., Chen, A., Guo, Z., Yan, M., Wu,

354   H., Yu, Z., 2016. Treatment of landfill leachate using immobilized Phanerochaete

355   chrysosporium loaded with nitrogen-doped TiO2 nanoparticles. J Hazard Mater.301, 106-

356   18.

357 19. Huang, C Y., Hu, KH., Wei, Z H., 2016. Comparison of cell behavior on pva/pva-gelatin

358   electrospun nanofibers with random and aligned configuration. Sci. Rep. 6, 37960. DOI:

359   10.1038/srep37960

360 20. Imran, M., Haider, S., Ahmad, K., Mahmood, A., Al-Masry, W A., 2013. Fabrication and

361   characterization of zinc oxide nanofibers for renewable energy applications. Arab. J.

362   Chem. 10, 1067-1072.

363 21. Jia, C., Batterman, S., 2010. A critical review of naphthalene sources and exposures

364   relevant to indoor and outdoor air. Int. J. Environ. Res. Publ. Health. 7, 2903-39.

365 22. Judy, I., Wu, C., Mo, Y., Evangelista, F A., von Ragué Schleyer, P., 2012. Is

366   cyclobutadiene really highly destabilized by antiaromaticity. Chemical Communications.

367   48, 8437-9.

368 23. Karak, T., Bhattacharyya, P., Paul, R K., Das, DK., 2013. Metal accumulation,

369   biochemical response and yield of Indian mustard grown in soil amended with rural

370   roadside pond sediment. Ecotoxicol Environ Saf. 92, 161-73.

371 24. Lair, A., Ferronato, C., Chovelon J M., Herrmann, J M., 2008. Naphthalene degradation

372   in water by heterogeneous photocatalysis, an investigation of the influence of inorganic

373   anions. J. Photochem. Photobiol A, Chem. 193,193-203.

374 25. Li, D., Nie, W., Chen, L., Miao, Y., Zhang, X., Chen, F., Yu, B., Ao, R., Yu, B., He, C.,

375   2017. Fabrication of curcumin-loaded mesoporous silica incorporated polyvinyl

376   pyrrolidone nanofibers for rapid hemostasis and antibacterial treatment. RSC Adv. 7,

377   7973-82.

378 26. Li, J., Zhao, F., Zhang, L., Zhang, M., Jiang, H., Li, S., Li, J., 2015. Electrospun hollow

379   ZnO/NiO heterostructures with enhanced photocatalytic activity. RSC Adv.5, 67610-6.

380 27. Liang, Y., Guo, N., Li, L., Li, R., Ji, G., Gan, S., 2015. Preparation of porous 3D Ce-

381   doped ZnO microflowers with enhanced photocatalytic performance. RSC Adv. 5,

382   59887-94.

383 28. Lin, D., Wu, H., Zhang, R., Pan, W., 2009. Enhanced photocatalysis of electrospun Ag–

384   ZnO hetero structured nanofibers. Chem. Mater. 21, 3479-84.

385 29. Liu, H., Yang, J., Liang, J., Huang, Y., Tang, C., 2008. ZnO nanofiber and nanoparticle

386   synthesized through electrospinning and their photocatalytic activity under visible light.

387   J. Am. Ceram. Soc. 91, 1287-91.

388 30. Liu, L., Liu, Z., Bai, H., Sun, D D., 2012. Concurrent filtration and solar photocatalytic

389   disinfection/degradation using high-performance Ag/TiO 2 nanofiber membrane. Water

390   Res. 46, 1101-12.

391 31. Luo, Z H., Wei, C L., He, N N., Sun, Z G., Li, H X., Chen, D., 2015. Correlation between

392   the photocatalytic degradability of PAHs over Pt/TiO 2-SiO$_2$ in water and their

393   quantitative molecular structure. J. Nanomater.6. http://dx.doi.org/10.1155/2015/284834

394 32. Mahmoodi, N M., Mokhtari-Shourijeh, Z., 2015.Preparation of PVA-chitosan blend

395   nanofiber and its dye removal ability from colored wastewater. Fibers and Polymers.

396   16,1861-9.

397 33. Malwal, D., Gopinath, P., 2016. Enhanced photocatalytic activity of hierarchical three

398   dimensional metal oxide@ CuO nanostructures towards the degradation of Congo red

399   dye under solar radiation. Catal. Sci. Technol. 6, 4458-72.

400 34. Malwal, D., Gopinath, P., 2017. Efficient adsorption and antibacterial properties of

401   electrospun CuO-ZnO composite nanofibers for water remediation. J. Hazard. Mater.

402   321, 611-21.

403 35. Mishra, S., Ahrenkiel, S P., 2012. Synthesis and characterization of electrospun

404   nanocomposite TiO 2 nanofibers with Ag nanoparticles for photocatalysis applications. J.

405   Nanomater. 16. http://dx.doi.org/10.1155/2012/902491

406 36. Mondal, K., 2017. Recent Advances in the Synthesis of Metal Oxide Nanofibers and

407   Their Environmental Remediation Applications. Inventions. 2, 9.

408   DOI:10.3390/inventions2020009

409 37. Mondal, K., Bhattacharyya, S., Sharma, A., 2014. Photocatalytic degradation of

410   naphthalene by electrospun mesoporous carbon-doped anatase TiO_2 nanofiber mats. Ind.

411   Eng. Chem. Res. 53, 18900-9.

412 38. Muthukumar, H., Gire, A., Kumari, M., Manickam, M., 2017. Biogenic synthesis of

413   nano-biomaterial for toxic naphthalene photocatalytic degradation optimization and

414   kinetics studies. Int. Biodeterior. Biodegrad. 119, 587-94.

415 39. Muthukumar, H., Pichiah, S., Leong, K H., Devi, S A., Manickam, M., 2017. Facile

416   Biosynthesis of ZnO and Iron Doped ZnO Nano-Catalyst, Physicochemical Traits and

417   Multifunctional Applications. J. Bionanoscience. 11,114-22.

418 40. Nair, M G., Nirmala, M., Rekha, K., Anukaliani, A., 2011. Structural, optical, photo

419   catalytic and antibacterial activity of ZnO and Co doped ZnO nanoparticles. Mater. Lett.

420   65,1797-800.

421 41. Panthi, G., Park, S J., Chae, S H., Kim, T W., Chung, H J., Hong, S T., Park, M., Kim, H

422   Y., 2017. Immobilization of Ag_3PO_4 nanoparticles on electrospun PAN nanofibers via

423 surface oximation, Bifunctional composite membrane with enhanced photocatalytic and

424 antimicrobial activities. J. Ind. Eng. Chem. 45, 277.

425 42. Park, J Y., Lee, I H., 2014. Photocatalytic degradation of 2-chlorophenol using Ag-doped

426 TiO 2 nanofibers and a near-UV light-emitting diode system. J. Nanomater. 1.

427 http://dx.doi.org/10.1155/2014/250803

428 43. Reddy, K R., Xie, T., Dastgheib, S., 2013. PAHs removal from urban storm water runoff

429 by different filter materials. J. Hazard. Toxic, Radioact. Waste. 18, 04014008.

430 44. Rezvani-Eivari, M., Amiri, A., Baghayeri, M., Ghaemi, F., 2016. Magnetized graphene

431 layers synthesized on the carbon nanofibers as novel adsorbent for the extraction of

432 polycyclic aromatic hydrocarbons from environmental water samples. J. Chromatogr. A.

433 1465, 1-8.

434 45. Samadi, M., Shivaee, H A., Zanetti, M., Pourjavadi, A., Moshfegh, A., 2012. Visible

435 light photocatalytic activity of novel MWCNT-doped ZnO electrospun nanofibers. J.

436 Mol. Catal. A, Chem. 359, 42-8.

437 46. Shahini, P., Ashkarran, A A., Hamidinezhad, H., Bahari, A., 2016. The role of iron

438 functionalization on the visible-light photocatalytic performance of TiO_2 nanofibers

439 suitable for environmental applications. Res. Chem. Intermed. 42, 8273-84.

440 47. Si, Y., Li, J., Zhao, C., Deng, Y., Ma, Y., Wang, D., Sun, G., 2017. Biocidal and

441 Rechargeable N-Halamine Nanofibrous Membranes for Highly Efficient Water

442 Disinfection. ACS Biomater. Sci. Eng. 3, 854-62.

443 48. Singh, P., Mondal, K., Sharma, A., 2013. Reusable electrospun mesoporous ZnO

444 nanofiber mats for photocatalytic degradation of polycyclic aromatic hydrocarbon dyes in

445 wastewater. J. colloid interface Sci. 394, 208-15.

446   49. Sood, S., Kumar, A., Sharma, N., 2016. Photocatalytic and Antibacterial Activity Studies

447   of ZnO Nanoparticles Synthesized by Thermal Decomposition of Mechano chemically

448   Processed Oxalate Precursor. Chemistry Select. 1, 6925-32.

449   50. Viswanathamurthi, P., Bhattarai, N., Kim, HY., Lee, DR., 2003. The photoluminescence

450   properties of zinc oxide nanofibres prepared by electrospinning. Nanotechnology. 15,

451   320.

452   51. Wan, J., Zeng, G., Huang, D., Hu, L., Xu, P., Huang, C., Deng, R., Xue, W., Lai, C.,

453   Zhou, C., Zheng, K., 2018. Rhamnolipid stabilized nano-chlorapatite: Synthesis and

454   enhancement effect on Pb-and Cd-immobilization in polluted sediment. J Hazard Mater.

455   343, 332-9.

456   52. Wan, J., Zhang, C., Zeng, G., Huang, D., Hu, L., Huang, C., Wu, H., Wang, L., 2016.

457   Synthesis and evaluation of a new class of stabilized nano-chlorapatite for Pb

458   immobilization in sediment. J Hazard Mater.320, 278-88.

459   53. Wang, J., Chen, Z., Chen, B., 2014. Adsorption of polycyclic aromatic hydrocarbons by

460   graphene and graphene oxide nanosheets. Environ. Sci. Technol. 48, 4817-25.

461   54. Wang, J., Liu, C., Li, J., Luo, R., Hu, X., Sun, X., Shen., Han, W., Wang, L., 2017. In-

462   situ incorporation of iron-copper bimetallic particles in electrospun carbon nanofibers as

463   an efficient Fenton catalyst. Appl. Catal., B, Environmental. 207, 316-25.

464   55. Wang, X W., Zhong, N N., Hu, D M., Liu, Z Z., Zhang, Z H., 2009. Polycyclic aromatic

465   hydrocarbon (PAHs) pollutants in groundwater from coal gangue stack area,

466   characteristics and origin. Wat Sci Tech. 59, 1043-51.

467   56. Wang, Y., Cheng, J., Yu, S., Alcocer, E J., Shahid, M., Wang, Z., Pan, W., Synergistic

468   effect of N-decorated and Mn^{2+} doped ZnO nanofibers with enhanced photocatalytic

469   activity. Sci. Rep. 2016, 6, 32711.

470   57. Zelinkova, Z., Wenzl, T., 2015. The occurrence of 16 EPA PAHs in food–a review.

471   Polycycl Aromat Compd. 35, 248-84.

472

473

474

475

476

477

478

479

480

List of FIGURES

Figure 1.
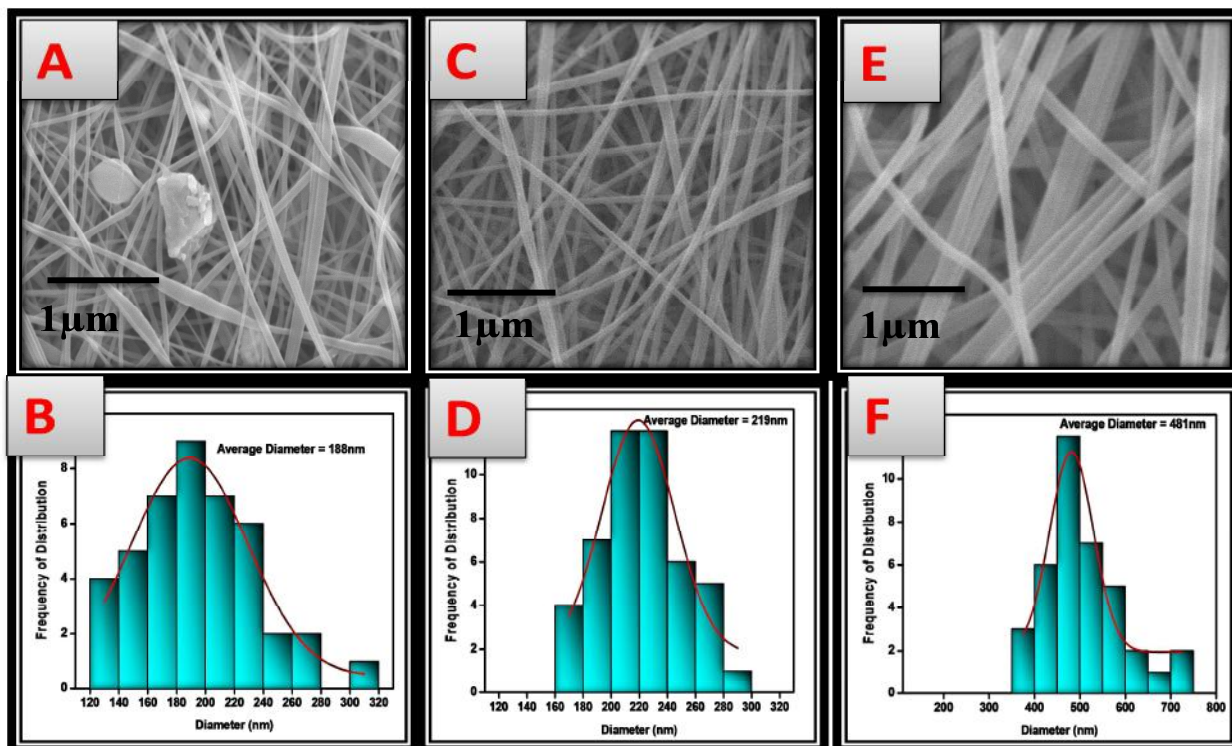
Fig. 1 SEM images and diameter distribution histograms of electrospun NFs with different PVA concentration and fixed 4 wt% Fe-doped ZnO NPs: (A and B) - 4wt% of PVA NFs, (C and D) - 8wt % of PVA NFs, and (E and F) -12wt % of PVA NFs.

Figure 2.
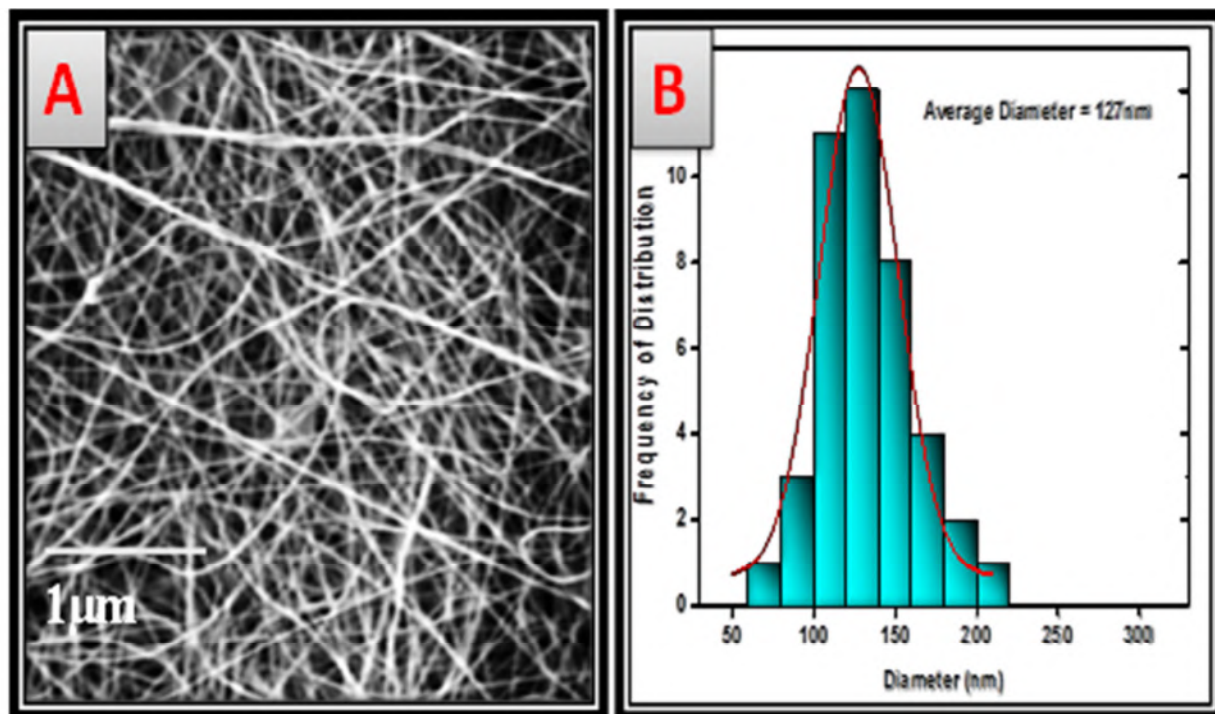
Fig. 2 SEM image and diameter distribution histogram of calcined 4 wt% of Fe-doped ZnO NFs.

Figure 3.
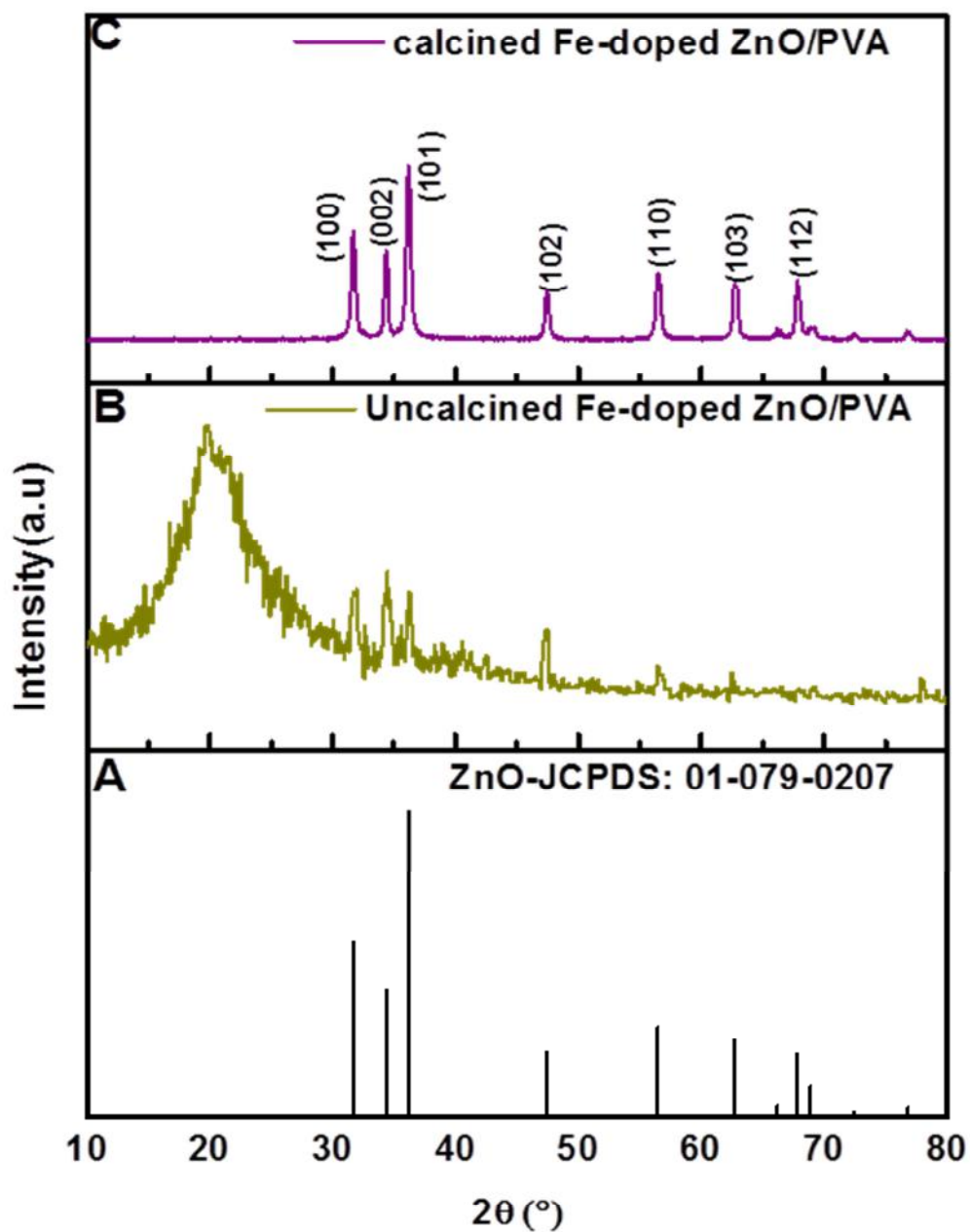
Fig. 3 XRD patterns of before and after calcination 4 wt% Fe-doped ZnO/PVA NFs

Figure 4.
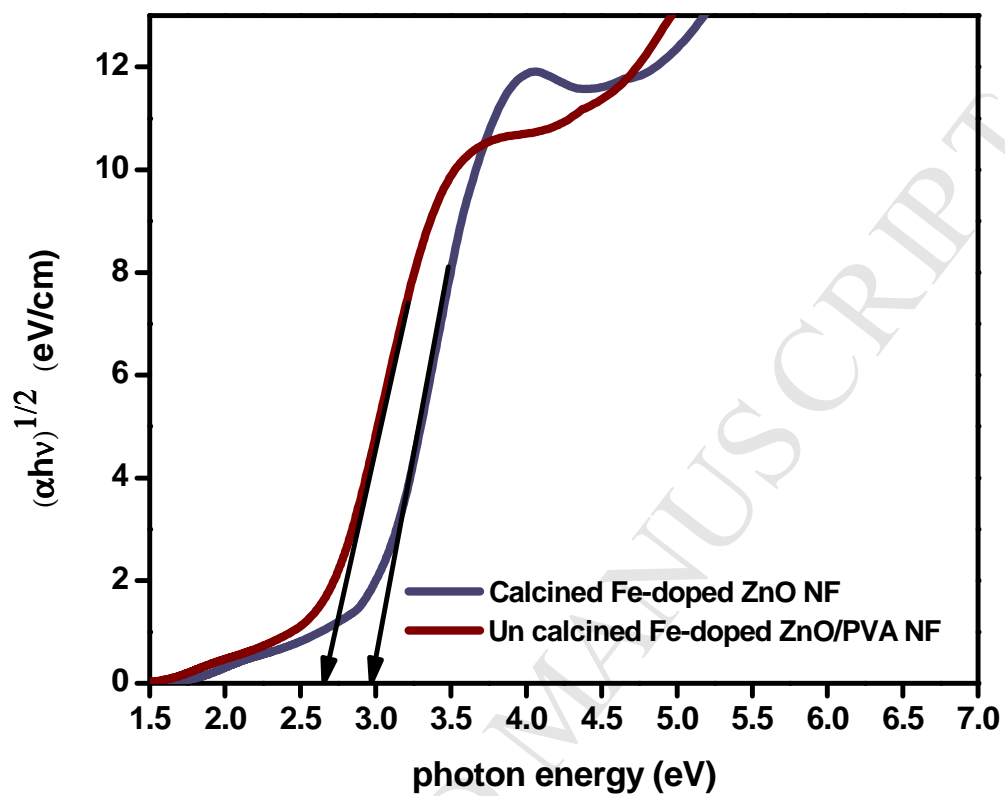
Fig. 4 Tauc plot of before and after calcination Fe-doped ZnO nanofibers for band gap calculation

Figure 5.
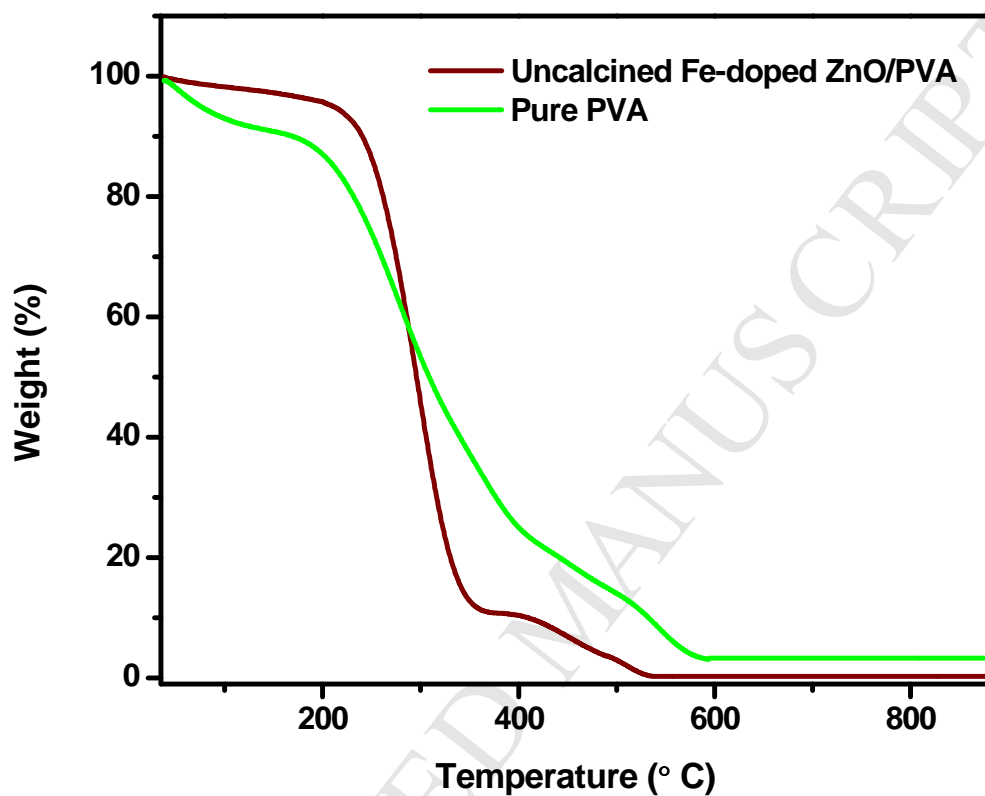
Fig. 5 TGA patterns of pure 8 wt % PVA nanofiber and Un-calcined 4 wt% Fe-doped ZnO/PVA nanofiber.

Figure 6.
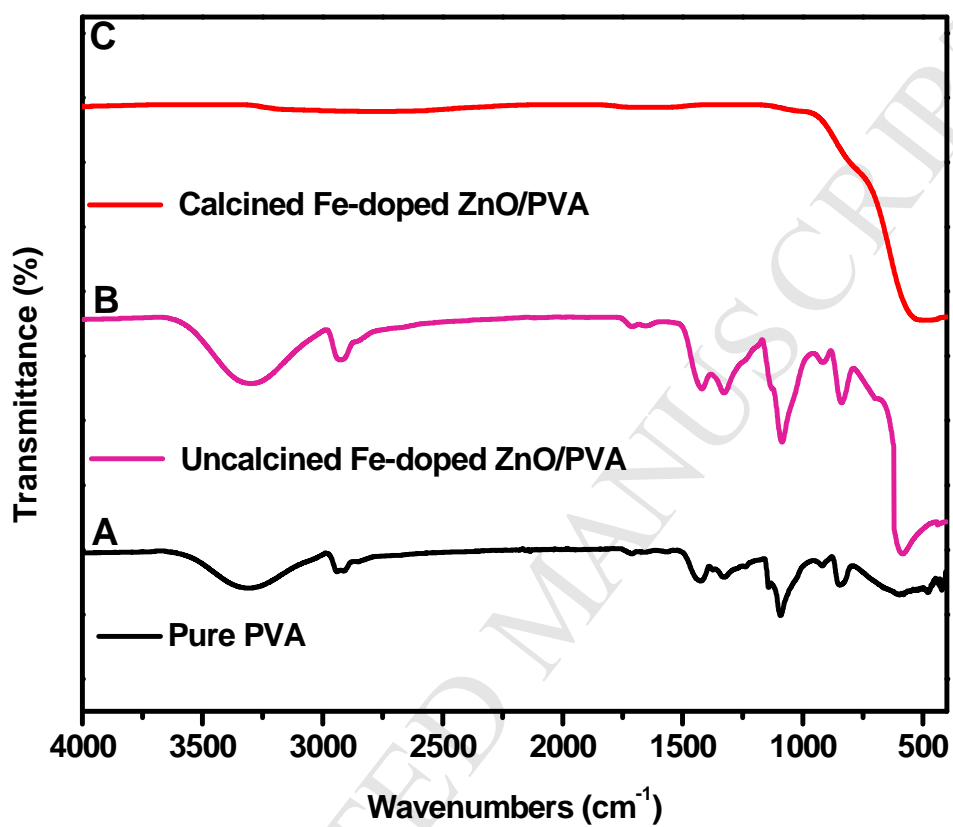
Fig. 6 IR spectra of pure 8 wt % PVA NF, before and after calcination 4 wt% Fe-doped ZnO/PVA NF

Figure 7.
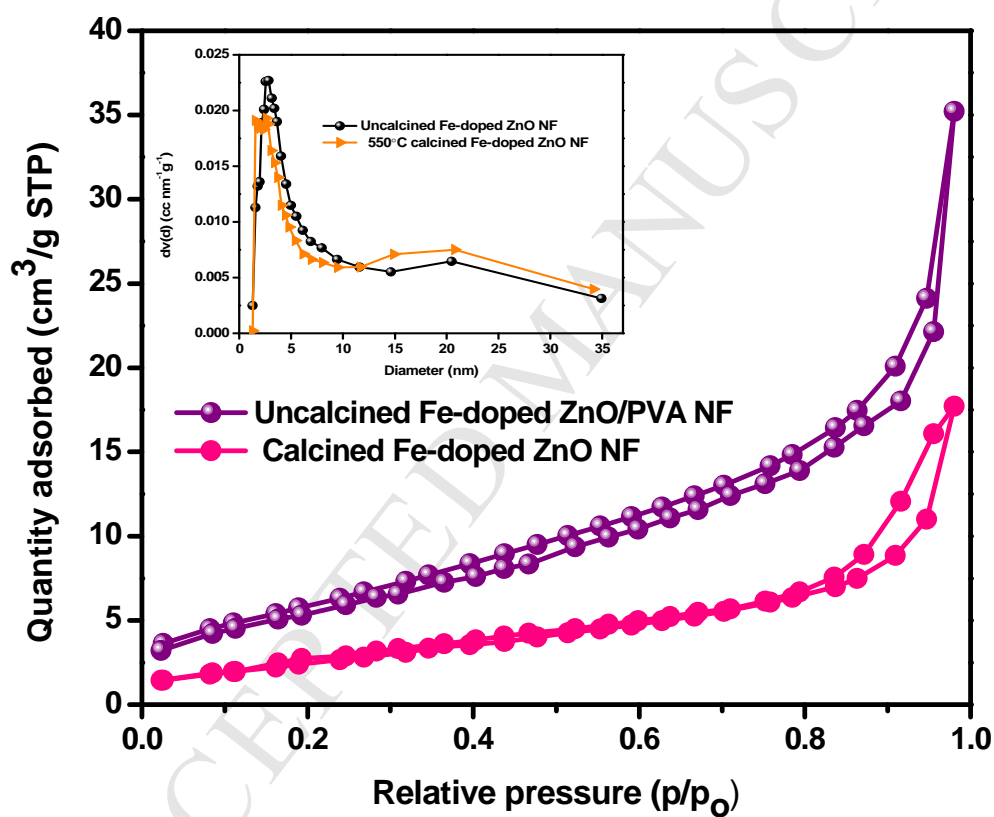
Fig. 7 Nitrogen adsorption – desorption isotherms and the corresponding pore size distribution (inset) curves of Calcined and Un-calcined Fe-doped ZnO/PVA nanofiber.

Figure 8.
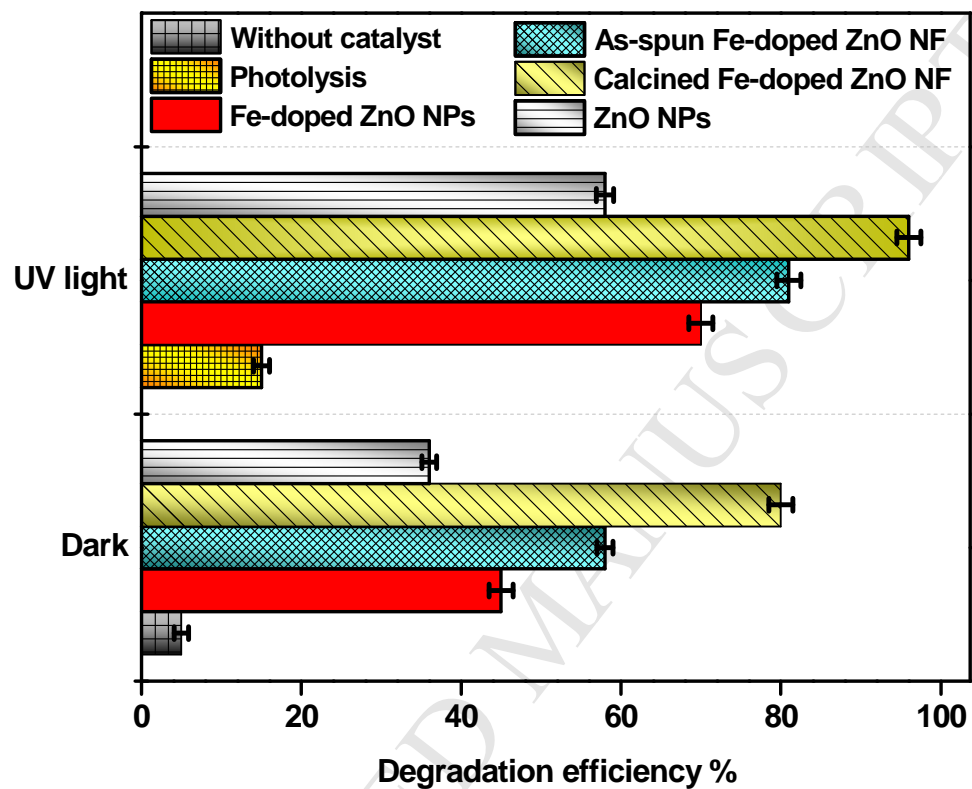
Fig. 8 Photocatalytic degradation of 40ppm of naphthalene using 60 ppm of catalyst under UV light

Figure 9.
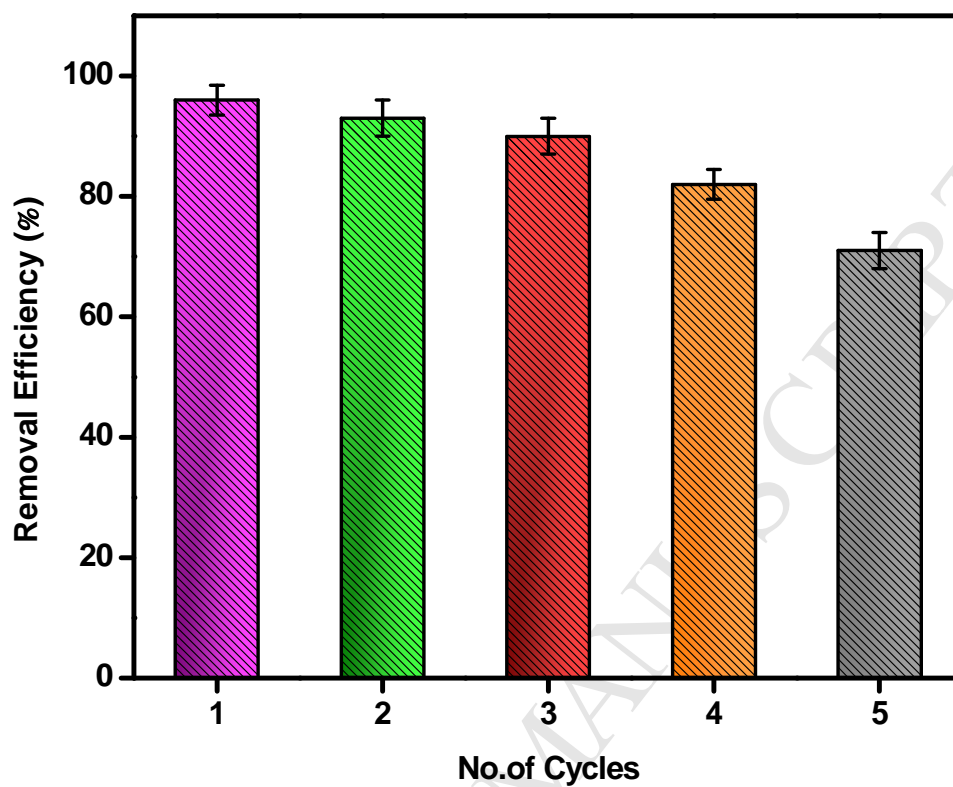
Fig. 9 Recyclability studies of calcined 4wt % Fe-doped ZnO nanofibers for the photocatalytic degradation of naphthalene